minerals

MDPI

Article

Silician Magnetite from the Copiapó Nordeste Prospect of Northern Chile and Its Implication for Ore-Forming Conditions of Iron Oxide–Copper–Gold Deposits

Elías González [1,2,*], Shoji Kojima [1], Yoshihiko Ichii [3], Takayuki Tanaka [2], Yoshikazu Fujimoto [2] and Takeyuki Ogata [4]

1 Departamento de Ciencias Geológicas, Universidad Católica del Norte, Av. Angamos 0610, Antofagasta, Chile; skojima@ucn.cl
2 Minera Nittetsu Chile Ltda., O´Higgins 744, Oficina 607, Copiapó, Chile; tanaka@mineranittetsu.cl (T.T.); fujimoto@mineranittetsu.cl (Y.F.)
3 Nittetsu Mining Consultants Co. Ltd., 2-3, Shiba 4-Chome, Minato-ku, Tokyo 108-0014, Japan; ichii_yoshihiko@nmconsults.co.jp
4 International Center for Research & Education on Mineral & Energy Resources, Akita University, 1-1 Tegata-Gakuen Machi, Akita 010-8502, Japan; take-ogt@gipc.akita-u.ac.jp
* Correspondence: eliasgonzalez@mineranittetsu.cl; Tel.: +56-52-2209800

Received: 20 September 2018; Accepted: 9 November 2018; Published: 14 November 2018

Abstract: Silica-bearing magnetite was recognized in the Copiapó Nordeste prospect as the first documented occurrence in Chilean iron oxide–copper–gold (IOCG) deposits. The SiO_2-rich magnetite termed silician magnetite occurs in early calcic to potassic alteration zones as orderly oscillatory layers in polyhedral magnetite and as isolated discrete grains, displaying perceptible optical differences in color and reflectance compared to normal magnetite. Micro-X-ray fluorescence and electron microprobe analyses reveal that silician magnetite has a significant SiO_2 content with small amounts of other "impure" components, such as Al_2O_3, CaO, MgO, TiO_2, and MnO. The oscillatory-zoned magnetite is generally enriched in SiO_2 (up to 7.5 wt %) compared to the discrete grains. The formation of silician magnetite is explained by the exchange reactions between 2Fe (III) and Si (IV) + Fe (II), with the subordinate reactions between Fe (III) and Al (III) and between 2Fe (II) and Ca (II) + Mg (II). Silician magnetite with high concentrations of SiO_2 (3.8–8.9 wt %) was similarly noted in intrusion-related magmatic–hydrothermal deposits including porphyry- and skarn-type deposits. This characteristic suggests that a hydrothermal system of relatively high-temperature and hypersaline fluids could be a substantial factor in the formation of silician magnetite with high SiO_2 contents.

Keywords: silician magnetite; Copiapó Nordeste; iron oxide–copper–gold deposit; micro-X-ray fluorescence; electron probe microanalysis

1. Introduction

Magnetite is a common oxide mineral in various types of ore deposits associated with high-temperature magmatic to low-temperature superficial conditions. In recent years, detailed chemical compositions of magnetite, particularly minor and trace elements, have been obtained from the principal types of magnetite deposits and serve as discriminating indicators [1–4]. In the Chilean Andes, magnetite is the predominant mineral in iron oxide–apatite (IOA) and iron oxide–copper–gold (IOCG) deposits. Although the genetic aspects of the former still remain uncertain, the latter is regarded as hydrothermal metasomatic in origin [4,5].

The Copiapó Nordeste IOCG deposit, with its abundant massive magnetite ores, is a new prospect in Northern Chile. These ores show a variety of modes of occurrence and textures, including martitization and pseudomorphic magnetite (mushketovite). In particular, optically different, orderly oscillatory layers are found in several polyhedral magnetite crystals, and their compositional peculiarities were elucidated using X-ray and electron microprobe analyses. It was revealed that the oscillatory-zoned magnetite contains significant amounts of SiO_2, Al_2O_3, CaO, and MnO. The silica contents are particularly high compared to those of other components, up to ~7.5 wt %. In the present study, we report on the mode of occurrence, paragenesis, optical properties, and detailed chemical compositions of Copiapó Nordeste magnetite, using a reflected-light microscope, micro-X-ray fluorescence (μ-XRF) spectrometry, and electron microprobe (EPMA) analysis. The chemical data obtained are compared with those of magnetite from other IOA and skarn-type deposits, with the objective to elucidate the characteristics of chemical substitution of the SiO_2-bearing magnetite termed "silician magnetite" [6–8] and IOCG ore-forming conditions deduced from its chemical compositions.

2. Geologic Framework

The Copiapó Nordeste prospect is situated approximately 45 km northeast of the city of Copiapó Chile (27°01′ S, 70°06′ W) and is part of the Early Cretaceous volcanic arc [9–12] (Figure 1). The volcanic arc has a N–S direction with a >700 km horizontal intra-arc extension and includes the Manto Verde and Candelaria IOCG deposits and also magnetite-rich IOA deposits [13]. Most of the deposits are distributed along the Atacama Fault Zone running in an NNW to NNE direction (Figure 1), which is regarded as a sinistral strike–slip fault system formed during transtensional oblique subduction [13]. The Copiapó Nordeste prospect is located on the eastern edge of the Early Cretaceous volcanic arc, and is hosted in the Punta del Cobre Formation composed predominantly of Early Cretaceous volcanic–volcaniclastic rocks. The mineralized zone mainly occurs in altered andesitic pyroclastic rocks in the upper levels of the formation, near the overlying Bandurrias Formation. A hornblende-bearing diorite porphyry, which is located ~1 km south of the prospect, intrudes into the Punta del Cobre and Bandurrias formations.

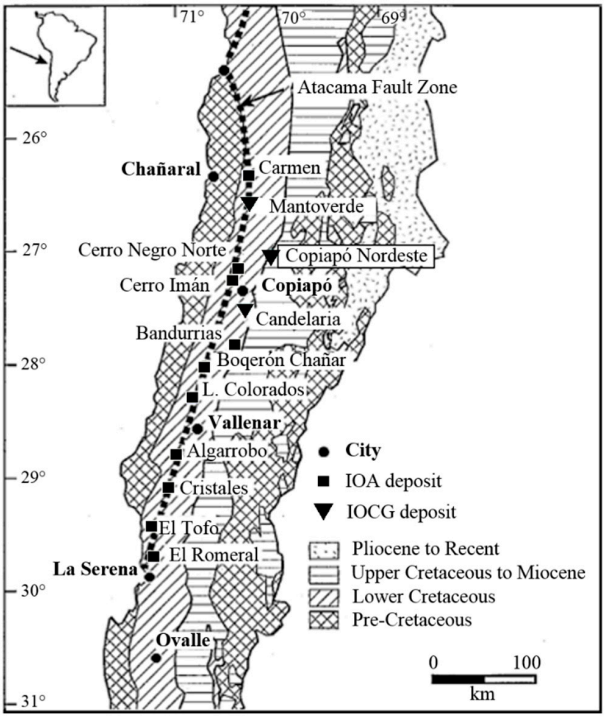

Figure 1. Simplified geologic map and location of the Copiapó Nordeste prospect in northern Chile, modified from Espinoza [9] and Marschik and Fontboté [12].

An initial metasomatic event of sodic–calcic alteration with earlier albitization and later actinolite is clearly observed in earlier breccia zones of the host rock. This zone is transversely overprinted by potassic alteration represented by K-feldspar. The alteration occurs pervasively with the Fe–oxide mineralization, and also in veinlets with the principal sulfide minerals. The dominant hydrothermal alteration in the deposit is chloritization, and nearly the entire host rocks are subjected to the alteration with sulfide mineralization. At a later stage, calcite veinlets crosscut the altered host rocks, locally replacing the preexistent chalcopyrite–hematite veinlets.

The Copiapó Nordeste IOCG deposit is characterized by a superficial Cu–oxide zone and deeper Cu–Fe sulfide zone, and the primary mineralization of magnetite occurs extensively in both zones as massive strata, veins, breccia fillings, and aggregates. The mineralized zones contain subordinate amounts of specular hematite and Cu–Fe–sulfide minerals, such as pyrite, chalcopyrite, and bornite, with lesser amounts of chalcocite, digenite, and supergene covellite.

3. Analytical Methods

Seventeen representative core and surface samples were collected and their polished sections were studied under a BX-51 type Olympus reflected-light polarizing microscope to examine the modes of occurrence and paragenesis of the magnetite. Magnetite samples with anomalous optical properties and characteristic textures (Nos. C-4, C-10, S-2) were selected for the detailed micro-X-ray fluorescence and electron microprobe analyses.

Qualitative micro-X-ray fluorescence analyses were performed using a Bruker M4 TORNADO-type instrument (Bruker, Billerica, MA, USA) with Rh target at the University of Católica del Norte (UCN), Chile. The instrument has an energy-dispersive X-ray spectroscopy (EDS) system that enables the detection of lower concentrations of elements than traditional SEM–EDS, thus allowing the entire energy spectra of all elements with higher atomic numbers than Na [14]. Operating conditions included: 50 kV X-ray beam energy, 100 μA specimen current, 19.9 mbar sample chamber pressure, 20 μm spot size, with 20 ms per pixel, and distance between spot size of 25 μm.

Quantitative chemical analyses were carried out using a JEOL JXA-8530F-type field emission-electron microprobe analyzer (JEOL, Akishima, Japan) in the conventional wavelength dispersion method at the Institute for Mining Research and Studies, Akita Prefecture, Japan. Magnetite compositions were measured with a constant beam-diameter of 1 μm under 15 kV and 20 nA conditions. The standards used were from the JEOL material collections and include: Si and Al (Al_2SiO_5), Mg (Mg_2SiO_4), Ti and Mn ($MnTiO_3$), Cr (Cr_2O_3), Ca and V ($Ca_3(VO_4)_2$), Fe (synthetic hematite), Cu (Cu metal), Ni (NiO), and Co (CoO). Curved crystals employed were LiF (Cr, Fe, Ni, Co), LiFH (Mn, V), TAP (Si, Al, Mg), PET (Cu), PETH (Ca), and PETJ (Ti), and the weight ratios were computed using the conventional ZAF method [6–8]. Mean detection limits of 0.01 wt % were achieved except for Fe–Kα (0.02 wt %), based on counting statistics. Furthermore, nearly all analytical results were mapped in EPMA–backscattered electrons (BSE) images.

4. Analytical Results

4.1. Microscopic Descriptions

Magnetite is the most abundant mineral, normally occurring as fine-grained massive aggregates in association with Cu–Fe–sulfide minerals. Magnetite also occurs as layers, veins, and breccias and is locally replaced by later hematite (martitization) (Figure 2a). Pseudomorphic replacement of magnetite occurs in early-formed specular hematite (so-called "mushketovite") [12,15], as shown in Figure 2b. Polyhedral grains of magnetite in the earlier calcic alteration zone locally exhibit orderly oscillatory-zoned structures parallel to external crystal faces (Figure 2c,d), which can be detected by differences in color and reflectance. The anomalous zones can be differentiated from the martitization that occurs in fractures, crystal margins, and along cleavages. As shown in Figure 2c,d, thin layered zones are more grey-colored and show lightly lower reflectance, in comparison to normal magnetite.

Its polishing hardness is nearly equal to that of normal magnetite, as no distinct relief is observed between the grey-colored zones and the optically normal magnetite. The grey-colored phase also occurs as isolated discrete grains in the potassic alteration zone and may be confused with normal magnetite, due to their similar optical properties [6]. Martitization is also found in the polyhedral magnetite grains with the oscillatory-zoned structure, and it appears that the hematite replacement is preferentially in the optically normal magnetite layers (Figure 2c,d).

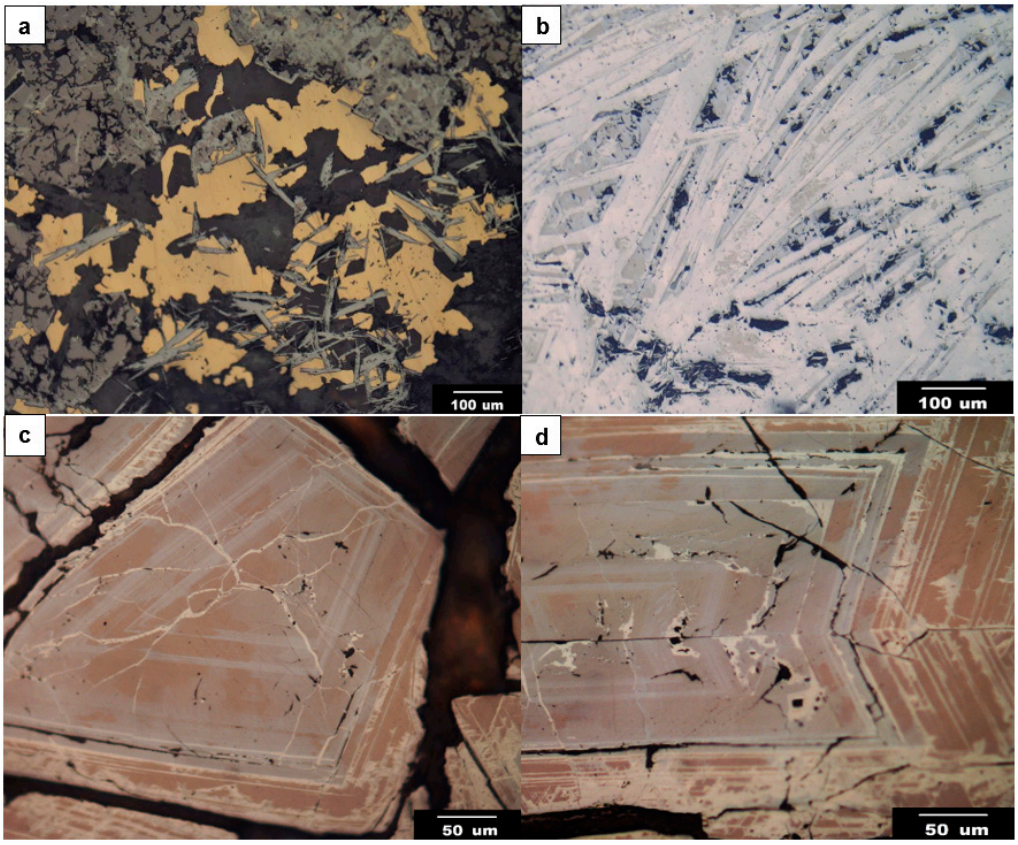

Figure 2. Photomicrographs of characteristic iron–oxide minerals in the Copiapó Nordeste prospect under reflected light: (**a**) Partially-martitized normal magnetite associated with chalcopyrite and specular hematite. (**b**) Coarse-grained columnar hematite with muschketovic magnetite. (**c**,**d**) Polyhedral magnetite with orderly oscillatory-zoned structure of silician (grey-colored) and optically normal (brownish colored) magnetite cut by hematite veinlets (whitish color).

Hematite is also a common mineral and is observed in the mineralized veins and breccias in frequent association with magnetite and Cu–Fe sulfides. The following two stages of hematite occurrences are observed: An early-formed phase of coarse-grained columnar aggregates with partial mushketovic replacement, and a late-formed phase of fine-grained specular hematite associated intimately with chalcopyrite and martitized polyhedral magnetite (Figure 2a).

Pyrite and chalcopyrite are intimately associated and occur as disseminations, aggregates, and veinlets. Chalcopyrite partially replaces pyrite margins, and rounded pyrite relicts are sporadically isolated in a chalcopyrite matrix. A minor proportion of the Cu sulfides is represented by bornite, chalcocite–digenite, and covellite as hypogene and supergene phases. Bornite occurs normally as irregular aggregates associated with chalcopyrite grains and laminae, which are regarded as intergrown and exsolution products, respectively. Chalcocite occurs as both hypogene and supergene phases, and the latter more rarely fills magnetite grains. Small amounts of digenite as a hypogene phase occur closely associated with bornite and supergene covellite. The paragenetic sequence of the aforementioned ore minerals and its relation to alteration minerals is summarized in Figure 3.

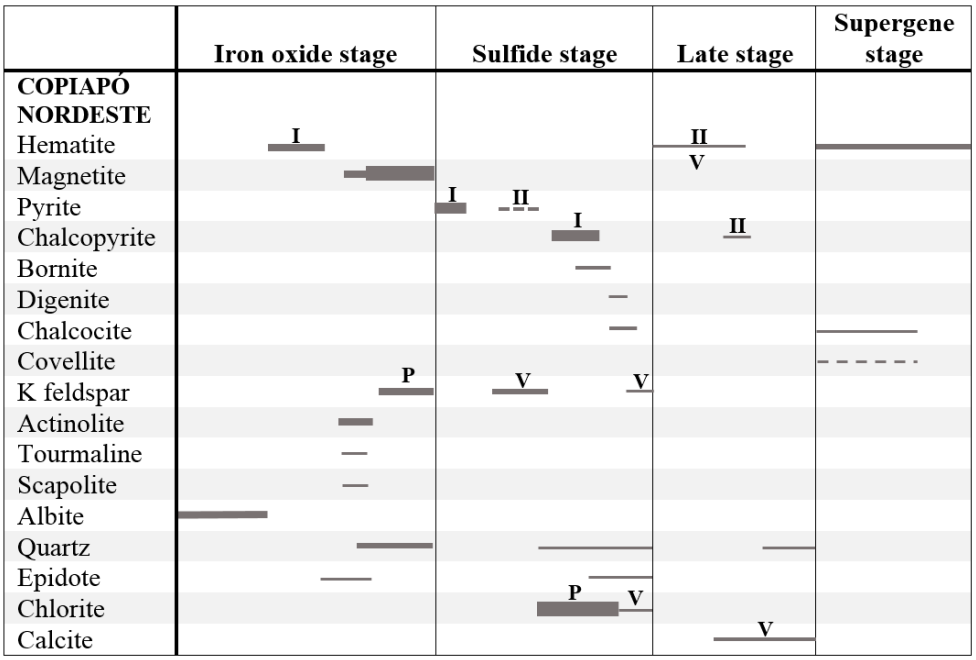

Figure 3. Paragenetic sequence of ore and alteration minerals in the Copiapó Nordeste prospect. The Roman numerals indicate mineralization stages. Abbreviations: P = pervasive alteration; V = vein and veinlet.

4.2. Micro-X-ray Fluorescence Analysis

Qualitative analyses were performed on the distinct magnetite samples: Oscillatory-zoned magnetite (No. S-2), isolated discrete magnetite (No. C-4), and mushketovitic magnetite (No. C-10). The analytical results (Figure 4) identified such elements as Si, Al, K, Ca, Ti, Cr, and Mn, disregarding the Rh–L-radiation originating from the target material and diffraction peak near 4.8 keV caused by Brägg reflection [14]. These compositional characteristics indicate that the magnetite corresponds to Type 2 classified by Shimazaki [8]: Magnetite with appreciable amounts of Al_2O_3, MgO, CaO, and other components, along with SiO_2. There is a clear chemical difference between the isolated discrete and oscillatory-zoned magnetite. In the former, the above named elements are generally detected in lower levels less than 1 cps/eV. By contrast, the latter shows markedly elevated levels up to ~5 cps/eV. The important peaks are for Si, Ca, Ti, and Mn, which show approximately positive relations, particularly in the Si–Ca pair.

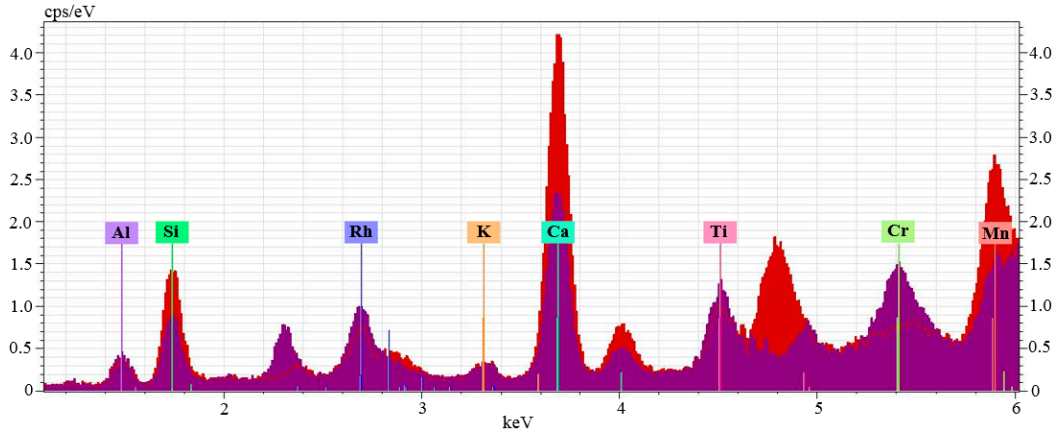

Figure 4. Micro-X-ray fluorescence spectra patterns of orderly oscillatory-zoned (red) and isolated discrete (purple) magnetite. See text for detailed explanations.

4.3. EPMA

Prior to quantitative EPMA, qualitative checking was made for the grey-colored oscillatory layers zoned with optically normal magnetite (No. S-2) and the isolated discrete magnetite grains (No. C-4). The following elements were appreciably detected, and were thus measured: Fe, Si, Al, Ti, V, Mn, Mg, Ca, Cu, Ni, and Co. Some elements not detected in the micro-X-ray fluorescence analyses were discerned, but K was under the detection limit. A total of 94 quantitative point analyses were carried out for the two samples, and their representative analytical results are listed in Table 1. Due to the Fe-calculation as FeO (II) in the measurements, the total weight of all the oxide components was usually around ~93%, which led to reasonable recalculated values [7,8,16].

The magnetite analyzed contains, in the order of percent SiO_2, up to ~7.5 wt % in the oscillatory-zoned magnetite and to ~2.8 wt % in the discrete grey-colored magnetite. Some analytical points with their SiO_2 contents are mapped in the EPMA–BSE images (Figure 5). Appreciable amounts of Al_2O_3 ($\leq$2.1 wt %), CaO, and MgO and lesser amounts of TiO_2 and MnO are also contained in the two types of magnetite, in contrast to normal magnetite. Such distinct characteristics are clearly represented in the oscillatory-zoned sample, with widely-scattered ranges of the "impure" elements. Compared to the oscillatory-zoned magnetite, the discrete magnetite grains display more limited compositional ranges in all of the "impure" elements (Table 1). The positive correlation between Si and Ca observed in the micro-X-ray fluorescence analysis is also detected in the EPMA data. The CaO contents of silician magnetite tend to increase with increasing SiO_2 contents, ranging up to 1.29 wt %.

Several compositional trends between the components measured (FeO, Fe_2O_3, SiO_2, Al_2O_3, CaO + MgO) were observed; Fe_2O_3 clearly shows a negative correlation with SiO_2 and Al_2O_3 (Figure 6a,b), whereas FeO and CaO + MgO displays a positive correlation with SiO_2 (Figure 6c,d). Negative correlations between Fe^{3+} and Si^{4+} and between Fe^{3+} and Al^{3+} were also reported in several skarn-type Fe deposits [16,17].

The average compositions of "impure" elements in the two samples (C-4, S-2) are plotted in the discriminant diagrams of Al + Mn vs. Ti + V, Ca + Al + Mn vs. Ti + V, and Ni/(Cr + Mn) vs. Ti + V (Figure 7), published by Dupuis and Beaudoin [1], in order to compare with data of silician magnetite from other types of Fe deposits [17–20]. The mean value of the fairly homogeneous C-4 sample plots within the IOCG field; however, that of the zoned S-2 sample plots in the skarn field. This implies that the Copiapó Nordeste silician magnetite has a chemical characteristic between IOCG- and skarn-types.

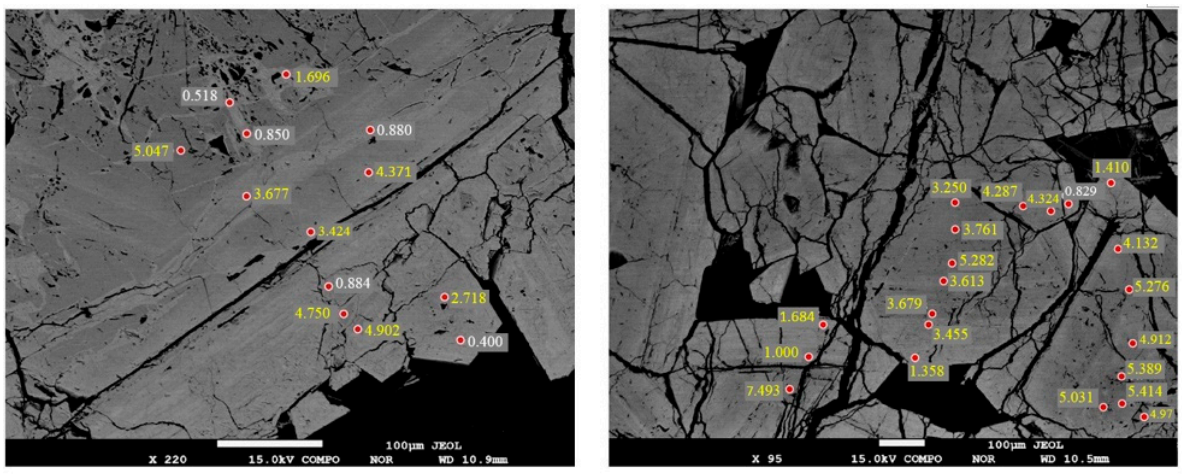

(**a**) (**b**)

Figure 5. EPMA–backscattered electrons (BSE) images for oscillatory-zoned magnetite with Si contents (wt %). The yellow and white values indicate SiO_2 > 1% and SiO_2 > 1%, respectively. (**a**,**b**) The Si contents are variable within the magnetite crystals and the lower contents are observed in martititized zones.

Table 1. Electron microprobe (EPMA) selected results of orderly oscillatory-zoned (S-2) and discrete grey-colored (C-4) magnetite.

No.	S2-1	S2-2	S2-3	S2-4	S2-5	S2-6	S2-7	S2-8	S2-9	S2-10	C4-1	C4-2	C4-3	C4-4	C4-5	C4-6	C4-7
SiO_2	0.23	0.40	0.71	1.45	4.75	5.05	5.17	5.28	5.41	7.49	0.08	0.09	0.59	1.31	2.07	2.36	2.79
TiO_2	0.00	0.03	0.05	0.11	0.19	0.08	0.22	0.00	0.24	0.06	0.03	0.02	0.03	0.01	0.05	0.08	0.10
Al_2O_3	0.07	0.05	0.06	0.69	1.34	1.11	1.10	0.68	1.63	2.10	0.17	0.11	0.25	0.10	0.29	0.19	0.19
Cr_2O_3	0.01	0.02	0.06	0.00	0.07	0.00	0.02	0.01	0.00	0.29	0.02	0.00	0.02	0.02	0.05	0.00	0.06
V_2O_3	0.01	0.00	0.01	0.49	0.12	0.00	0.00	0.03	0.00	0.03	0.00	0.05	0.04	0.00	0.00	0.00	0.00
FeOt *	92.35	91.58	92.02	89.70	85.57	86.13	85.55	86.85	85.26	82.06	92.99	93.01	92.70	91.57	89.99	88.96	88.97
MnO	0.04	0.06	0.00	0.61	0.19	0.09	0.11	0.16	0.06	0.21	0.02	0.07	0.07	0.00	0.00	0.00	0.07
MgO	0.02	0.11	0.00	0.15	0.84	0.56	0.73	0.12	0.83	1.24	0.02	0.00	0.03	0.18	0.53	0.60	0.49
CaO	0.00	0.00	0.00	0.26	0.95	1.05	1.16	0.47	1.29	0.76	0.00	0.00	0.02	0.28	0.47	0.72	0.76
CuO	0.07	0.07	0.01	0.00	0.00	0.06	0.11	0.00	0.00	0.44	0.01	0.00	0.01	0.02	0.03	0.02	0.12
NiO	0.00	0.02	0.06	0.00	0.01	0.07	0.02	0.00	0.00	0.20	0.06	0.00	0.02	0.00	0.00	0.00	0.00
CoO	0.11	0.12	0.17	0.00	0.06	0.06	0.15	0.13	0.10	0.14	0.20	0.19	0.16	0.15	0.17	0.20	0.09
Total	92.90	92.46	93.14	93.46	92.56	94.26	94.33	93.74	94.82	95.00	93.59	93.54	93.95	93.64	93.64	93.14	93.63
Fe_2O_3	68.11	67.35	66.83	64.26	55.56	55.33	54.83	54.10	53.79	50.49	68.85	68.83	67.61	65.96	63.88	62.93	62.03
FeO	31.06	30.98	31.88	32.44	35.58	36.35	36.22	38.17	36.85	36.63	31.04	31.08	31.87	32.23	32.51	32.34	33.16
Total	99.73	99.21	99.84	100.46	99.67	99.81	99.82	99.16	100.21	100.06	100.49	100.43	100.72	100.25	100.04	99.44	99.85

* Total Fe as FeO, and is recalculated into FeO and Fe_2O_3, as shown in the second block.

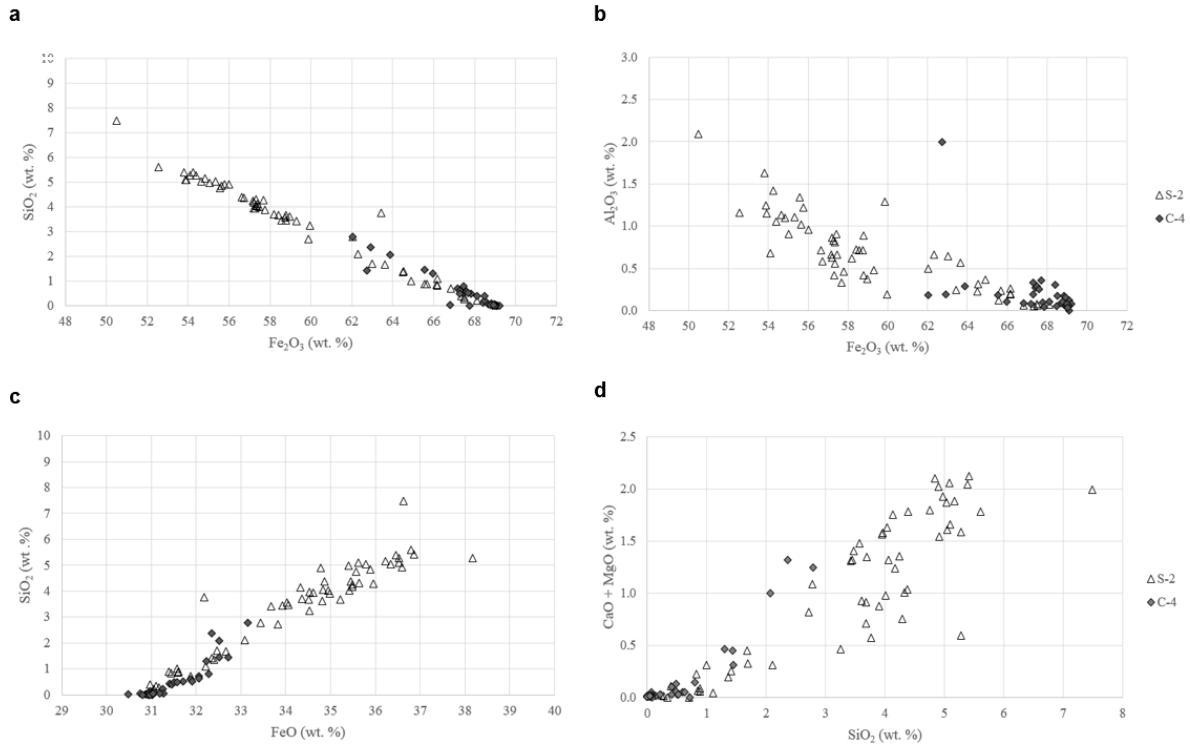

Figure 6. Correlative relations between detected components (FeO, Fe_2O_3, Al_2O_3, Ca + Mg) of silican magnetite: (**a**) Fe_2O_3 vs. SiO_2, (**b**) Fe_2O_3 vs. Al_2O_3, (**c**) FeO vs. SiO_2, and (**d**) (CaO + MgO) vs. SiO_2. See text for detailed explanations.

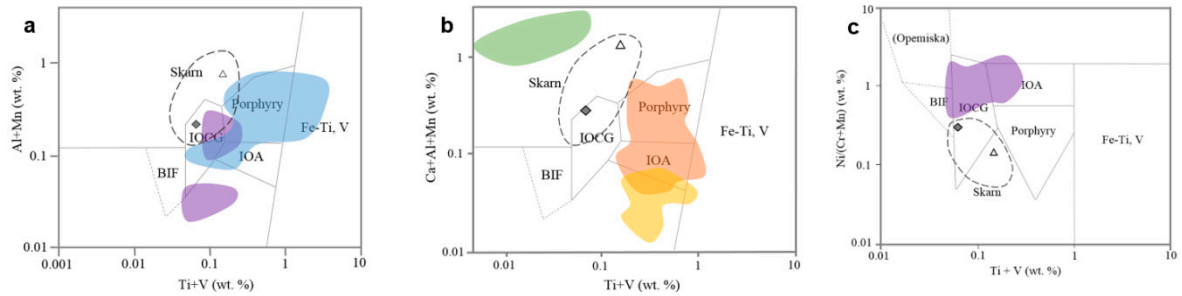

Figure 7. Average minor element compositions of orderly oscillatory-zoned magnetite (△) and discrete grey-colored magnetite (◆) plotted in the discriminant diagrams of (**a**) Al + Mn vs. Ti + V, (**b**) Ca + Al + Mn vs. Ti + V, and (**c**) Ni/(Cr + Mn) vs. Ti + V. Data from the approximate range of samples from Copiapó Nordeste (dotted line circle), Los Colorados (blue) [4], El Laco (purple) [19], Chadormalu Si-rich magnetite (orange) [20], Chadormalu Si-poor magnetite (yellow) [20], and Chengchao (green) [17]. Modified from Dupuis and Beaudoin [1] and Nadoll et al. [3]. See text for detailed explanations.

5. Discussion

5.1. Substitution Chemistry in Magnetite and Martitization

The magnetite structure follows an inverse spinel, with O^{2-} ions forming a face-centered cubic lattice and iron cations occupying interstitial sites. Fe^{2+} cations are observed to occupy half of the octahedral lattice sites, and alternatively Fe^{3+} cations occupy the other octahedral lattice sites and all of the tetrahedral lattice sites [21]. In the case of silician magnetite, the replacement of Fe^{3+} in the

tetrahedral site by Si^{4+} and the electrostatically-compensating substitution of Fe^{3+} by Fe^{2+} [6–8,21] can be assumed as follows:

$$[Fe^{3+}][Fe^{2+}, Fe^{3+}] \leftrightarrow [Si^{4+}][Fe^{2+}, Fe^{2+}] \ (2Fe^{3+} \rightleftharpoons Si^{4+} + Fe^{2+}). \quad (1)$$

This substitution is clearly shown in Figure 6a,c. Furthermore, Figure 6b,d suggests that the following substitutions additionally occur in minor ranges:

$$[Fe^{3+}][Fe^{2+}, Fe^{3+}] \leftrightarrow [Al^{3+}][Fe^{2+}, Fe^{3+}] \ (Fe^{3+} \rightleftharpoons Al^{3+}), \quad (2)$$

$$[Si^{4+}][Fe^{2+}, Fe^{2+}] \leftrightarrow [Si^{4+}][Fe^{2+}, Ca^{2+} + Mg^{2+}] \ (2Fe^{2+} \rightleftharpoons Ca^{2+} + Mg^{2+}). \quad (3)$$

The ionic radii of Ca^{2+}, Fe^{2+}, and Mg^{2+} in the octahedral site are estimated to be 100 pm, 77 pm, and 72 pm, respectively [3,22]; namely, they are in the relation $Ca^{2+} > Fe^{2+} > Mg^{2+}$. Thus, such a coupled substitution could be incidentally induced in the formation of silician magnetite. As stated earlier, silician magnetite is found in the calcic alteration zone, and the phase is also enriched in CaO. This relation means that the calcic alteration played an important role in the formation of CaO-rich silician magnetite.

The chemical data imply that silician magnetite is a member of solid solution of Fe_3O_4 and γ- Fe_2SiO_4 [8]. Shimazaki [8] suggests that silician magnetite is rather a product of solid solution with a maghemite-like structure, because the Mössbauer data for a similar silician magnetite of a Japanese skarn-type deposit indicate the presence of ferrous cation vacancy in the octahedral site. Ohkawa et al. [16], using X-ray powder diffraction analyses, revealed that the silician magnetite of another Japanese skarn deposit is not maghemite, but magnetite. Considering all these results, it is suitably defined that silician magnetite is an "impure" element-bearing magnetite.

As described in the former section, martitization selectively occurs in optically normal magnetite layers in the polyhedral zoned grains (Figure 2c,d). Huberty et al. [23] made a similar observation in the Hamersley BIF microbands, in which only magnetite with low SiO_2 was transformed into hematite. This selective oxidation means that the SiO_2 impurity constrains the transformation of magnetite into hematite.

5.2. Comparison with Other Deposits

As shown in Figure 7, silician magnetite from the Copiapó Nordeste has an intermediate chemical characteristic between skarn- and IOCG-type deposits. In the (Al + Mn) vs. (Ti + V), (Ca + Al + Mn) vs. (Ti + V), and Ni/(Cr + Mn) vs. (Ti + V) diagrams, previously published data of silician magnetite from other types of deposits, IOA (Los Colorados, El Laco, Chadormalu) and skarn-type (Chengchao), are displayed. The applied data are limited to primary hydrothermal silician magnetite with no dissolution–reprecipitation textures [17,18]. The oscillatory-zoned magnetite from the brecciated diorite of the Los Colorados deposit shows a large elemental dispersion in the (Al + Mn) vs. (Ti + V) diagram, and the data extend into the Porphyry, IOA, IOCG, and Fe–Ti areas [4]. The zoned magnetite of the El Laco deposit exhibits particularly variable ranges in the (Al + Mn) vs. (Ti + V) and Ni/(Cr + Mn) vs. (Ti + V) diagrams, extending over the IOCG, IOA, and Porphyry areas [19]. The compositionally-zoned magnetite of the Chadormalu deposit spreads over distinct areas [20]; the silica-rich magnetite is enriched in Ca + Al + Mn contents in comparison with silica-poor magnetite, occupying mainly the Porphyry and IOA areas. By contrast, the Chengchao skarn magnetite is totally included within the Skarn area and is characterized by high (Ca + Al + Mn) and low (Ti + V) contents. Furthermore, it is noted that the primary magnetite from the Chengchao deposit is relatively silica-rich (<3.2 wt %). Considering these features on silician magnetite, the Copiapó Nordeste samples are regarded to display an intermediate chemical characteristic between the Skarn and Porphyry–IOA zones.

Nadoll et al. [3] and Deditius et al. [24] suggested that (Al + Mn) and (Ti + V) values tend to become lower with decreasing temperature. If this tendency is applicable to general temperature ranges of

IOCG deposits, the oscillatory-zoned silician magnetite formed at a slightly higher temperature than discrete grey-colored magnetite.

5.3. Magnetite Ore-Forming Condition

The aforementioned substitution of Fe^{2+} for Fe^{3+} in the octahedral site of silician magnetite and its close association with pyrrhotite led Shiga [7] to propose that silician magnetite was formed under reducing conditions. A similar discussion was made by Huberty et al. [23], who investigated low-temperature silician magnetite in the Hamersley banded iron formation (BIF). They suggested that the presence of organic carbon yields the reducing conditions necessary to stabilize silician magnetite at low temperatures. By contrast, Shimazaki [8] insisted that oxidation states have no obvious relation to its formation, because no systematic variation of silica contents is demonstrated with the oxidation state estimated from associated Fe minerals (pyrrhotite–pyrite to hematite). As shown in Figure 3, the Copiapó Nordeste magnetite occurs in the relatively high-temperature calcic to potassic alteration zones, and any associated minerals suggestive of reducing conditions are not observed in all the mineralization stages. Thus, the formation of silician magnetite is considered to have occurred under relatively high-temperature conditions with variable oxidation states.

Silician magnetite occurs in various types of ore deposits with high- to low-temperature conditions, as summarized by Huberty et al. [23] and Xu et al. [25], including porphyry-type [26], skarn-type [6–8,16–18,27,28], banded iron formation (BIF) [23,25], and volcanic-related massive sulfide [29]. The highest value of SiO_2 content in magnetite (~8.9 wt %) is recognized in a porphyry-type deposit [26]. Moreover, skarn-type deposits show a higher frequency in the appearance of silician magnetite and have considerably high SiO_2 contents, ranging from 3.2 to 6.5 wt % [6–8,16,17,27,28]. The two types are generally defined as intrusion-related magmatic–hydrothermal deposits involving relatively high-temperature and high-salinity fluids [30]. The silician magnetite of the Copiapó Nordeste could be the first documented occurrence in Chilean IOCG-type deposits. Similar to the porphyry- and skarn-type deposits, these types of deposits are generally regarded to also be related to high-temperature and hypersaline fluid-related hydrothermal systems, particularly in the earlier iron–oxide stage (e.g., [12,31]). It is well known that saline fluids increase the solubility of quartz at high temperatures above ~300 °C, changing the retrograde solubility of quartz at the approximate temperature range of 375–550 °C [32–34]. This effect could be a significant driving force to precipitate silician magnetite, in addition to the temperature effect in silica solubility. Considering all these features, we concluded that magnetite with high Si contents is a high-temperature product particular to magmatic–hydrothermal deposits.

6. Summary and Conclusions

As the first documented appearance in the IOCG deposits, silician magnetite was recognized in the Copiapó Nordeste prospect. Its characteristics obtained in this study are summarized as follows:

1. Silician magnetite occurs in the calcic to potassic alteration stages as orderly oscillatory layers in polyhedral magnetite and isolated discrete grains. Silician magnetite is distinct in color and reflectance from normal magnetite, and can be optically distinguished with the reflecting microscope.
2. Qualitative and quantitative microanalyses show that silician magnetite contains significant amounts of SiO_2 with lesser contents of such "impure" components as Al_2O_3, CaO, MgO, TiO_2, and MnO. In general, oscillatory-zoned magnetite is richer in SiO_2 than the discrete grains, and the highest values of SiO_2 contents reach up to 7.5 wt % in the oscillatory layers and to 2.8 wt % in the discrete grains. The SiO_2 impurity prevents silician magnetite from undergoing martitization.
3. The formation of silician magnetite is represented by the substitutional reactions of $2Fe^{3+} \rightleftharpoons Si^{4+} + Fe^{2+}$, with the incidental reactions of $Fe^{3+} \rightleftharpoons Al^{3+}$ and $2Fe^{2+} \rightleftharpoons Ca^{2+} + Mg^{2+}$.

4. Silician magnetite from the Copiapó Nordeste has no dissolution–reprecipitation texture, and displays an intermediate chemical characteristic between the skarn and porphyry–IOA deposits in the previously published discrimination diagrams.
5. Silician magnetite occurs in a wide variety of types of ore deposits from high-temperature porphyry- and skarn-type to low-temperature BIF. The higher contents of SiO_2 (3.8–8.9 wt %) are noted in the intrusion-related magmatic–hydrothermal deposits, including the IOCG-type. These types of deposits are considered to have been derived from relatively high-temperature and hypersaline fluids, which are responsible for the formation of silician magnetite with high SiO_2 contents.

Author Contributions: E.G. achieved the whole mineralogical descriptions and wrote this earlier manuscript, which was revised and translated by his teaching adviser S.K. All authors contributed to geological investigations. In particular, the senior geologists of the prospect, Y.I., T.T. and Y.F. elucidated its geologic framework, and supplied the magnetite samples studied with valuable suggestions. T.O. performed EPMA analyses of the magnetite samples.

Acknowledgments: This work was completed as part of the first author's graduate thesis. Part of the expenses of this study was covered by the Facultad de Ingeniería y Ciencias Geológicas and Departamento de Ciencias Geológicas of Universidad Católica del Norte, to which we express our sincere thanks. We wish to thank Andrew Menzies and Jorge García of Universidad Católica del Norte, who helped us in the micro-X-ray fluorescence analyses and the preparation of polished sections, respectively. We thank David Lentz of University of New Brunswick, Robert King of Universidad Católica de la Santisma Concepción, and three anonymous reviewers for their constructive suggestions.

Conflicts of Interest: The authors declare no conflict of interest.

References

1. Dupuis, C.; Beaudoin, G. Discriminant diagrams for iron oxide trace element fingerprinting of mineral deposit types. *Miner. Depos.* **2011**, *46*, 319–335. [CrossRef]
2. Dare, S.A.S.; Barnes, S.J.; Beaudoin, G.; Méric, J.; Boutroy, E.; Potvin-Doucet, C. Trace elements in magnetite as petrogenic indicators. *Miner. Depos.* **2014**, *49*, 785–796. [CrossRef]
3. Nadoll, P.; Angerer, T.; Mauk, J.L.; French, D.; Walshe, J. The chemistry of hydrothermal magnetite: A review. *Ore Geol. Rev.* **2014**, *61*, 1–32. [CrossRef]
4. Knipping, J.; Bilenker, J.; Simon, A.; Reich, M.; Barra, F.; Deditius, A.; Wälle, M.; Heinrich, C.; Holtz, F.; Munizaga, R. Trace elements in magnetite from massive iron oxide-apatite deposits indicate a combined formation by igneous and magmatic-hydrothermal processes. *Geochim. Cosmochim. Acta* **2015**, *171*, 15–38. [CrossRef]
5. Williams, P.J.; Barton, M.; Johnson, D.A.; Fontboté, L.; de Haller, A.; Mark, G.; Oliver, N.H.S.; Marschik, R. Iron-oxide copper-gold deposits: Geology, space-time distribution, and possible models of origin. In *Economic Geology*; 100th Anniversary Volume; Society of Economic Geologists, Inc.: Littleton, CO, USA, 2005; pp. 371–405.
6. Shiga, Y. Silician magnetite from the Kamaishi mine, Japan. *Min. Geol.* **1988**, *38*, 437–440.
7. Shiga, Y. Further study of silician magnetite. *Min. Geol.* **1989**, *39*, 305–309.
8. Shimazaki, H. On the occurrence of silician magnetites. *Resour. Geol.* **1998**, *48*, 23–29. [CrossRef]
9. Espinoza, S. The Atacama-Coquimbo ferrifereous belt, northern Chile. In *Stratabound Ore Deposits in the Andes*; Society for Geology Applied to Mineral Deposits Special Publication 8; Springer: Berlin/Heidelberg, Germany, 1990; pp. 395–412.
10. Lara, L.; Godoy, E. Hoja Quebrada Salitrosa, Región de Atacama. Servicio Nacional de Geología y Minería. *Mapas Geol.* **1998**, *76*, 30. (In Spanish)
11. Arévalo, C. Carta Copiapó, Región de Atacama. Servicio Nacional de Geología y Minería. *Carta Geol. Chile* **2005**, *91*, 54. (In Spanish)
12. Marschik, R.; Fontboté, L. The Candelaria-Punta del Cobre iron oxide Cu-Au (-Zn-Ag) deposits, Chile. *Econ. Geol.* **2001**, *96*, 1799–1826.
13. Sillitoe, R.H. Iron oxide-copper-gold deposits: An Andean view. *Miner. Depos.* **2003**, *38*, 787–812. [CrossRef]

14. Haschke, M.; Boehm, S. Micro-XRF in Scanning Electron Microscopes. In *Advances in Imaging and Electron Physics*; Peter, W., Hawkes, W., Eds.; Elsevier: Amsterdam, The Netherlands, 2017; pp. 1–60.
15. Ramdohr, P. *The Ore Minerals and Their Intergrowths*; Pergamon Press: Oxford, UK, 1980; p. 1207.
16. Ohkawa, M.; Miyahara, M.; Ohta, E.; Hoshino, K. Silicon-substituted magnetite an accompanying iron oxides and hydroxides from the Kumano mine, Yamaguchi Prefecture, Japan: Reexamination of the so-called maghemite (γ-Fe_2O_3). *J. Mineral. Petrol. Sci.* **2007**, *102*, 182–193. [CrossRef]
17. Hu, H.; Li, J.W.; Lentz, D.; Ren, Z.; Zhao, X.F.; Deng, X.D.; Hall, D. Dissolution-reprecipitation process of magnetite from the Chengchao iron deposit: Insight into ore genesis and implication for *in-situ* chemical analysis of magnetite. *Ore Geol. Rev.* **2014**, *57*, 393–405. [CrossRef]
18. Hu, H.; Lentz, D.; Li, J.W.; McCarron, T.; Zhao, X.F.; Hall, D. Reequilibration processes in magnetite from iron skarn deposits. *Econ. Geol.* **2015**, *110*, 1–8. [CrossRef]
19. Broughm, S.G.; Hanchar, J.M.; Tornos, F.; Westhues, A.; Attersley, S. Mineral chemistry of magnetite from magnetite-apatite mineralization and their rocks: Examples from Kiruna, Sweden, and El Laco, Chile. *Miner. Depos.* **2017**, *52*, 1223–1244. [CrossRef]
20. Heidarian, H.; Lentz, D.; Alirezaei, S.; Peighambari, S. Using the chemical analysis of magnetite to constrain various stages in the formation and genesis of the Kiruna-type Chadormalu magnetite-apatite deposit, Bafq district, Central Iran. *Mineral. Petrol.* **2016**, *110*, 927–942. [CrossRef]
21. Lund, C.R.F.; Dumesic, J.A. Strong oxide-oxide interactions in silica-supported magnetite catalysis.1. X-ray diffraction and Mössbauer spectroscopy evidence for interaction. *J. Phys. Chem.* **1981**, *85*, 3175–3180. [CrossRef]
22. Shannon, R.D.; Prewitt, C.T. Effective ionic radii in oxides and fluorides. *Acta Crstallogr.* **1969**, *B25*, 925–945. [CrossRef]
23. Huberty, J.M.; Konishi, H.; Heck, P.R.; Fournelle, J.H.; Valley, J.W.; Xu, H. Silician magnetite from the Dales Gorge member of the Brockman iron formation, Hamersley Group, Western Australia. *Am. Mineral.* **2012**, *97*, 26–37. [CrossRef]
24. Deditius, A.P.; Reich, M.; Simon, A.; Suvorova, A.; Knipping, J.; Roberts, M.P.; Rubanov, A.; Saunders, M. Nanogeochemistry of hydrothermal magnetite. *Contrib. Mineral. Petrol.* **2018**, *173*, 46. [CrossRef]
25. Xu, H.; Shen, Z.; Konishi, H. Si-magnetite nano-precipitates in silician magnetite from banded iron formation: Z-contrast imaging and ab initio study. *Am. Mineral.* **2014**, *99*, 2196–2202. [CrossRef]
26. Imai, A. Generation and evolution of ore fluids for porphyry Cu-Au mineralization of the Santo Tomas II (Philex) deposit, Philippines. *Resour. Geol.* **2001**, *51*, 71–96. [CrossRef]
27. Shcheka, S.A.; Romanenko, I.M.; Chubarov, V.M. Silica bearing magnetite. *Contrib. Mineral. Petrol.* **1977**, *63*, 103–111. [CrossRef]
28. Wang, L.J.; Shimazaki, H.; Shiga, Y. Skarns and genesis of the Huanggang Fe-Sn deposit, Inner Mongolia, China. *Resour. Geol.* **2008**, *51*, 359–376. [CrossRef]
29. Westendorp, R.W.; Watkinson, D.H.; Jonasson, I.R. Silicon-bearing zoned magnetite crystals and the evolution of hydrothermal fluids at the Ansil Cu-Zn mine, Rouyn-Noranda, Quebec. *Econ. Geol.* **1991**, *86*, 1110–1114. [CrossRef]
30. Wilkinson, J.J. Fluid inclusions in hydrothermal ore deposits. *Lithos* **2001**, *55*, 229–272. [CrossRef]
31. Rieger, A.A.; Marschik, R.; Díaz, M. The evolution of the hydrothermal IOCG system in the Mantoverde district, northern Chile: New evidence from microthermometry and stable isotope geochemistry. *Miner. Depos.* **2012**, *47*, 359–369. [CrossRef]
32. Fournier, R.O. A method of calculating quartz solubilities in aqueous sodium chloride solutions. *Geochim. Cosmochim. Acta* **1983**, *47*, 579–586. [CrossRef]
33. Fournier, R.O. The behavior of silica in hydrothermal solutions. *Rev. Econ. Geol.* **1985**, *2*, 45–61.
34. Monecke, J.; Reynolds, T.J.; Tsuruoka, S.; Bennett, M.M.; Skews, W.B. Quartz solubility in the H_2O-NaCl systems: A framework for understanding vein formation in porphyry copper deposits. *Econ. Geol.* **2018**, *113*, 1007–1046. [CrossRef]